Loss of Hippocampal Calretinin and Parvalbumin Interneurons in the 5XFAD Mouse Model of Alzheimer's Disease

Naomi K. Giesers and Oliver Wirths (iD)

Abstract

The deposition of amyloid-β peptides in the form of extracellular plaques and neuronal degeneration belong to the hallmark features of Alzheimer's disease (AD). In addition, impaired calcium homeostasis and altered levels in calcium-binding proteins seem to be associated with the disease process. In this study, calretinin- (CR) and parvalbumin- (PV) positive gamma-aminobutyric acid-producing (GABAergic) interneurons were quantified in different hippocampal subfields of 12-month-old wild-type mice, as well as in the transgenic AD mouse models 5XFAD and Tg4-42. While, in comparison with wild-type mice, CR-positive interneurons were mainly reduced in the CA1 and CA2/3 regions in plaque-bearing 5XFAD mice, PV-positive interneurons were reduced in all analyzed subfields including the dentate gyrus. No reduction in CR- and PV-positive interneuron numbers was detected in the non-plaque-forming Tg4-42 mouse, although this model has been previously demonstrated to harbor a massive loss of CA1 pyramidal neurons. These results provide information about hippocampal interneuron numbers in two relevant AD mouse models, suggesting that interneuron loss in this brain region may be related to extracellular amyloid burden.

The hippocampus, a part of the brain with an important role in memory consolidation, is one of the most severely affected brain regions in Alzheimer's disease (AD), the most common form of dementia. Neuropathological alterations in the hippocampus in AD consist primarily of extracellular β-amyloid (Aβ) plaque deposition, the accumulation of neurofibrillary tangles composed of hyperphosphorylated tau protein, as well as marked neuronal loss and concomitant neuroinflammation (Selkoe, 2001). The degeneration of large pyramidal or projection neurons is one of the major neuropathological hallmarks of AD (Pearson et al., 1985).

In addition to pyramidal neurons, the hippocampus contains a subset of GABAergic cells, which can be classified by their immunoreactivity against calcium-binding proteins such as calretinin (CR) or parvalbumin (PV). These interneurons are scattered throughout all major hippocampal subfields and play important roles for cortical circuit function and regulation, although they represent only 10% to 15% of the overall neuronal population (Pelkey et al., 2017). CR-positive interneurons were shown to heavily innervate other cells such as calbindin-containing interneurons and are further characterized by features such as their frequent dendrodendritic and axodendritic contacts with each other (Gulyás et al., 1996). Throughout the entire brain, PV-expressing cells play roles in a variety of higher brain functions, including feedforward and feedback inhibition, pattern separation, and high-frequency network oscillations (Hu et al., 2014). They can be subdivided into groups targeting different domains of pyramidal cells, such as basket, axo-axonic, bistratified, or oriens-lacunosum-moleculare cells

Department of Psychiatry and Psychotherapy, Molecular Psychiatry, University Medical Center (UMG), Georg-August-University, Göttingen, Germany

Corresponding Author:
Oliver Wirths, Department of Psychiatry and Psychotherapy, Molecular Psychiatry, University Medical Center (UMG), Georg-August-University, Von-Siebold-Str. 5, 37075 Göttingen, Germany.
Email: owirths@gwdg.de

(Klausberger et al., 2005). In the hippocampus, these GABAergic interneurons play important roles in lateral inhibition in the dentate gyrus (DG; Espinoza et al., 2018) and mediate hippocampal–neocortical communication that is required for successful memory consolidation (Xia et al., 2017).

Immunohistochemical analysis of human AD brain samples demonstrated a significant loss (∼60%) of PV-positive interneurons in the DG/CA4 and CA1-CA2 subfields, while no obvious decline was observed in CA3, subiculum, or presubiculum (Brady and Mufson, 1997), as well as in the perirhinal cortex (Sanchez-Mejias et al., 2020) in comparison with control brains. Neurons containing distinct calcium-binding protein also seem to show differential vulnerability in AD, as PV-positive cells showed a clear atrophy with a diminished basket-like network in Layer II of the entorhinal cortex in AD patients, while CR-positive cells were well preserved in this area (Mikkonen et al., 1999). However, in, for example, the piriform cortex, a preferential vulnerability of CR-positive cells colocalizing with amyloid-β peptides was reported, while the prevalence of PV-positive was even increased in the AD cases (Saiz-Sanchez et al., 2015). Other studies employing human postmortem brain samples confirmed the differential vulnerability, as no overt differences were reported in, for example, visual cortex (Leuba et al., 1998) or superior frontal gyrus (Sampson et al., 1997).

The analysis of distinct interneuron populations in transgenic AD mouse models also yielded inconclusive results. While a variety of analyses reported a loss of PV- and CR-positive cells in hippocampal subfields in AD transgenic compared with age-matched control mice (Popović et al., 2008; Baglietto-Vargas et al., 2010; Takahashi et al., 2010; Albuquerque et al., 2015; Zallo et al., 2018), others found no genotype-dependent differences in, for example, the number CR-positive cells in the DG (Verdaguer et al., 2015).

In the present study, we performed a comprehensive analysis of CR- and PV-positive interneurons in the hippocampus of 12-month-old female 5XFAD (Oakley et al., 2006), Tg4-42 (Bouter et al., 2013), and age-matched wild-type (WT) control mice. While no hippocampal neuron loss has been described in 5XFAD mice (Jawhar et al., 2012), Tg4-42 mice harbor a significant loss of CA1 pyramidal neurons at this time point (Bouter et al., 2013). In our analysis, no alterations in the number of CR- and PV-positive interneurons were detected in the latter model; however, 5XFAD showed significantly diminished interneuron numbers in different hippocampal subfields, suggesting a relationship to the presence of robust extracellular amyloid pathology.

Material and Methods

Transgenic Mice

The generation of the 5XFAD mouse model (Tg6799) has been previously described (Oakley et al., 2006). Briefly, these mice overexpress the 695 amino acid isoform of the human amyloid precursor protein (APP) harboring the Swedish, Florida, and London mutations under the control of the neuron-specific murine Thy1-promoter. In addition, human presenilin-1 (PSEN1), carrying the M146L and L286V mutations, is expressed using the same promoter. 5XFAD mice used in the current study were backcrossed for more than 10 generations to C57Bl/6J WT mice (Jackson Laboratories, Bar Harbor, ME, USA) to generate an incipient congenic line on a C57Bl/6J genetic background (Jawhar et al., 2012).

The generation of the Tg4-42 mouse model has been previously described (Bouter et al., 2013). In brief, the Tg4-42 mouse model uses the murine Thy1-promoter to express the human Aβ4-42 peptide sequence. This peptide is fused to the thyrothropin-releasing hormone signal peptide sequence to ensure secretion through the secretory pathway. Only female mice were used for all genotypes in the present study, and the number of mice analyzed is given in the corresponding figures ($n = 5$–8). Analyses were carried out at 12 months of age, and both 5XFAD and T4-42 mice expressed the transgenes in a heterozygous fashion. All animals were maintained on a C57Bl/6J genetic background and handled according to German guidelines for animal care.

Immunohistochemistry

Mice were anesthetized and transcardially perfused with phosphate-buffered saline (PBS), followed by 4% paraformaldehyde in PBS, and brains were carefully dissected. The left brain hemisphere was postfixed in 4% paraformaldehyde and cryoprotected in a solution containing 30% sucrose in PBS. Tissues were quickly frozen on a dry ice plate and stored at –80°C until further processing. Next, the entire brain hemisphere was frontally cut into series of 30 μm thin sections using a cryostat (CM1850 UV, Leica, Germany). Every 10th section was systematically collected to obtain a series comprising the complete hemisphere (Cotel et al., 2008).

A series of every 10th coronal frozen section of 30 μm thickness was processed using a free-floating staining protocol to quantify the number of CR- and PV-positive interneurons. In brief, sections were rehydrated in PBS, followed by blockage of endogenous peroxidase activity using PBS including 0.3% hydrogen peroxide for 30 min. Following washing steps in PBS including 0.01% Triton X-100, unspecific antibody binding was blocked using PBS including 4% skim milk and 10% fetal

calf serum. The primary mouse monoclonal antibodies against CR (1:8000, Synaptic Systems, Göttingen, Germany; RRID:AB_2619906) and PV (1:4000, Synaptic Systems, RRID:AB_2619883) were incubated overnight, followed by incubation using anti-mouse-biotinylated secondary antibodies (DAKO, Glostrup, Denmark). Staining was visualized using the ABC method employing a Vectastain-Elite HRP Kit (Vector Laboratories, Burlingame, CA, USA). Diaminobenzidine (DAB) was used as chromogen providing a reddish-brown color, and counterstaining was carried out using hematoxylin.

Extracellular hippocampal amyloid plaque load was quantified in 5XFAD mice using paraffin-embedded right hemispheres. After initial deparaffinization in xylene and rehydration in a series of ethanol, sections were treated with 0.3% hydrogen peroxide in PBS to block endogenous peroxidases and antigen retrieval was achieved by boiling sections in 0.01 M citrate buffer pH 6.0, followed by 3 min incubation in 88% formic acid (Wirths et al., 2002). The slides were incubated with a pan-Aβ antibody detecting a central epitope (4G8, 1:1000, Signet Labs, RRID:AB_2313891) overnight, followed by anti-mouse-biotinylated antibody, and staining was visualized using the ABC method with a Vectastain-Elite HRP kit (Vector Laboratories, Burlingame, CA, USA) and DAB as chromogen. Plaque load was evaluated in CA1, CA2/3, and DG using an Olympus BX-51 microscope equipped with a Moticam Pro 282A camera (Motic) and the ImageJ software (V1.41, NIH, USA). Serial images of 100× magnification were captured on an average of three sections per animal. Using ImageJ, the pictures were binarized to 8-bit black-and-white images, and a fixed intensity threshold was applied defining the DAB staining.

Quantification of Neuron Numbers

Quantifications of CR- and PV-positive interneurons were carried out in the hippocampus (Bregma –1.1 to –3.8 mm), and cells were counted using a stereology workstation (Olympus BX51 with a motorized specimen stage for automatic sampling). The different hippocampal regions (CA1, CA2/3, DG) were delineated using 400× magnification, and neuron counting was performed at 1,000× magnification using the meander scan option of StereoInvestigator 7 (MBF Biosciences, Williston, USA) to quantify all CR- or PV-positive cells in a given section. The experimenter was blinded to genotype in all analyses. As every 10th section has been used for the quantitative analysis, the resulting number of immunopositive cells was multiplied by 10 to obtain the total number of CR- and PV-positive neurons (Gerberding et al., 2019). Data on CA1 neuron numbers and volume (Supplementary Figure 1) have been extracted and compiled from previous studies (Hüttenrauch, Brauss, et al., 2016; Hüttenrauch, Salinas, et al., 2016) using the same cohort of mice.

Statistical Analysis

Differences between groups were tested using one-way analysis of variance followed by Tukey's multiple comparison test. Data are given as mean $\pm$ standard deviation. All calculations were performed using GraphPad Prism version 8.4.1 for Windows (GraphPad Software, San Diego, CA, USA), and significance levels were given as follows: ***$p < .001$; **$p < .01$; *$p < .05$.

Results

To quantify the number of CR and PV immunoreactive cells, the hippocampus was divided into the three subfields CA1 (comprising the CA1 pyramidal cell layer, stratum oriens, stratum radiatum, and stratum lacunosum moleculare); CA2/3 (comprising stratum oriens and stratum lucidum); and DG (comprising molecular layer, granule cell layer, and hilus; Figure 1).

CR-Positive Interneurons

Analysis of CR-immunopositive cells in hippocampal subfields revealed a homogenous distribution. Intense immunoreactivity was detected at the inner part of molecular layer in the DG, as well as in interneuron somata in the hilus, with cell bodies in the granule cell layer being largely negative. In addition, CR-positive cells were detected in stratum radiatum and stratum lacunosum moleculare, as well as in the CA1 pyramidal cell layer (Figure 2).

The number of CR-positive interneurons was significantly reduced in the CA1 dorsal part (Bregma –2.7 to –3.8) in 5XFAD mice compared with WT and Tg4-42 ($p < .001$ and $p < .05$, respectively), resulting in significant reductions in the entire CA1 area in 5XFAD compared with WT and Tg4-42 ($p < .01$ and $p < .05$, respectively; Figure 3(A to C)). In the frontal CA2/3 region (Bregma –1.1 to –2.6), CR-positive cells were significantly reduced in 5XFAD compared with WT mice ($p < .05$); however, no alteration was detected in either the dorsal or entire CA2/3 region (Figure 3D to F). In the DG, numbers of CR-positive cells were unchanged (Figure 3G to I), and a combined analysis indicates a significant reduction in the entire hippocampus in 5XFAD compared with WT animals ($p < .05$; Figure 3J to L).

PV-Positive Interneurons

Intense labeling of PV-immunopositive cells was detected in the CA1 pyramidal cell layer, with the main immunoreactivity being present in processes. In the DG,
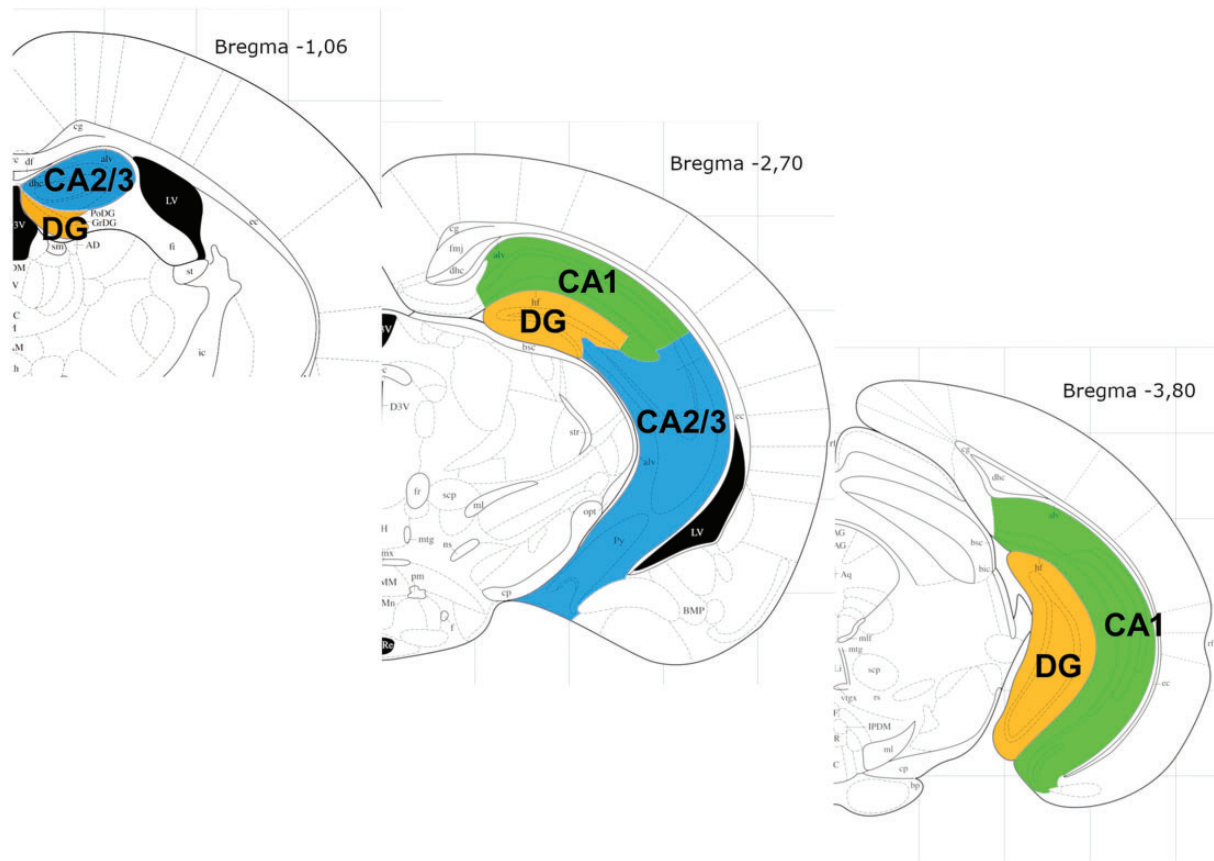
Figure 1. Schematic Presentation of the Counting Areas. CA1 (green), CA2/3 (blue), and DG (yellow) were quantified from Bregma −1.1 to −3.8. Figures were created using the mouse brain atlas by Paxinos and Franklin (2001).
DG = dentate gyrus.

prominent immunoreactivity was detected in distinct somata and processes of interneurons located in the granular cell layer and hilus (Figure 4).

Quantitative analyses of the number of PV-positive cells revealed a significant reduction in the dorsal part of the CA1 area in 5XFAD compared with WT and Tg4-42 mice (both $p < .01$), as well as in the entire CA1 ($p < .001$ and $p < .01$, respectively; Figure 5A to C). 5XFAD mice showed a significantly reduced number of PV-positive cells in the frontal CA2/3 region of the hippocampus compared with WT and Tg4-42 mice (both $p < .001$), resulting in a reduction of the overall PV-positive cell number in the entire CA2/3 region (5XFAD vs. WT, $p < .001$; 5XFAD vs. Tg4-42, $p < .01$; Figure 5D to F). While no changes were detected in the frontal part of the DG, again 5XFAD mice showed a significantly reduced PV-positive cell number compared with WT and Tg4-42 (both $p < .01$; Figure 5G to I). The combined analysis confirmed significantly reduced numbers of PV-positive interneurons in the entire hippocampal formation in the 5XFAD mouse model compared with WT and Tg4-42 (both $p < .001$; Figure 5J to L).

Amyloid Plaque Pathology

Immunohistochemical analyses of extracellular amyloid plaque deposition were carried out in the different hippocampal subfields of 12-month-old WT, Tg4-42, and 5XFAD mice. As expected due to the lack of mutant APP overexpression, no amyloid deposits were detected in either WT or Tg4-42 mice. In contrast, 5XFAD mice showed a considerable plaque load in the CA1 ($8.4 \pm 1.1\%$), CA2/3 ($6.4 \pm 0.9\%$), and DG ($11.4 \pm 3.2\%$) hippocampal subfields (Figure 6A to D).

Discussion

In the present report, we characterized the expression of the calcium-binding proteins CR and PV in the hippocampus of 12-month-old WT mice, as well as in the transgenic AD mouse models Tg4-42 and 5XFAD. The latter model represents a typical familial AD mouse model based on overexpression of mutant *APP* and *PSEN1* transgenes (Oakley et al., 2006). Aged 5XFAD mice show robust extracellular β-amyloid pathology and concomitant neuroinflammation in brain regions such as
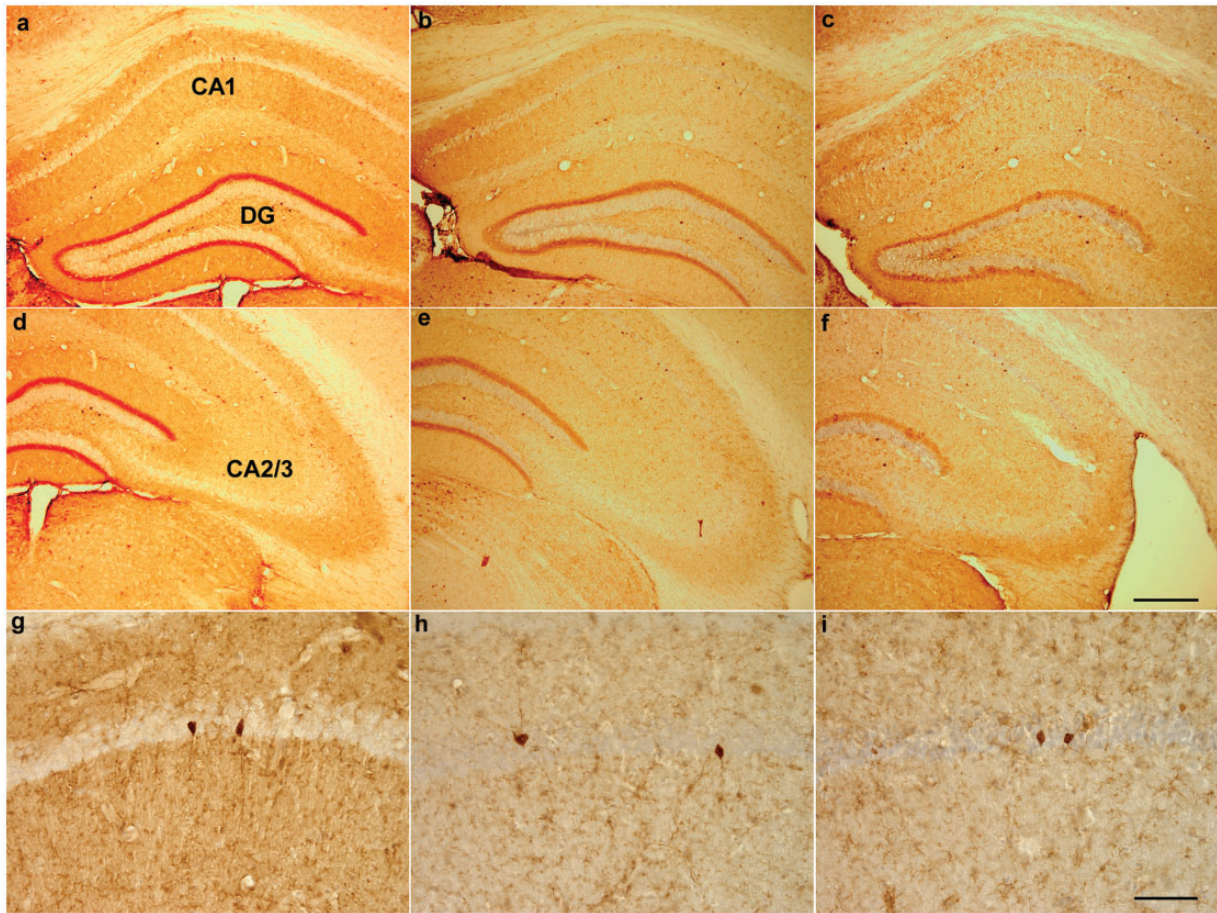
Figure 2. Distribution of calretinin (CR)-immunopositive cells within the hippocampal CA1, CA2/3, and DG subfields in 12-month-old WT (A, D), Tg4-42 (B, E), and 5XFAD mice (C, F). Higher magnifications of the CA1 layer in WT (G), Tg4-42 (H), and 5XFAD (I) mice. Scale bar: A to F: 200 μm; G to I: 50 μm.
DG = dentate gyrus.

cortex, thalamus, or hippocampus (Hüttenrauch et al., 2017), albeit in the absence of hippocampal CA1 neuron loss (Jawhar et al., 2012). In contrast, Tg4-42 mice lack overexpression of mutant human *APP* but express only Aβ4-42 peptides, an N-terminal truncated Aβ peptide variant that has been detected in high abundance in human AD brain (Portelius et al., 2010; Wirths and Zampar, 2019). While a massive loss of CA1 pyramidal neurons (>50%, Supplementary Figure 1) together with spatial and object recognition memory deficits, but without overt extracellular Aβ plaque pathology, is well documented in aged heterozygous Tg4-42 mice (Bouter et al., 2013; Hüttenrauch, Brauss et al., 2016), nothing is known about the potential involvement of hippocampal interneuron populations in the Tg4-42, as well as in the 5XFAD mouse model.

Previous studies analyzed the number of PV-positive GABAergic neurons in different regions of the frontal cortex of the 5XFAD mouse model. PV neuron density was reported to be significantly reduced in particular in deep cortical layers such as cingulate and secondary motor cortices (Ali et al., 2019), confirming data from others demonstrating an ∼30% reduction of PV-positive cell bodies in cortical Layer IV in 12-month-old 5XFAD mice (Flanigan et al., 2014). The observed significantly reduced number of both CR- and PV-positive cells in the hippocampus of 5XFAD mice is in line with results from other AD transgenic mouse models harboring substantial amyloidosis. In homozygous APP/ PS1ΔEx9 mice, decreased numbers of CR-, PV-, somatostatin-, or calbindin-positive interneurons have been described in the piriform and lateral entorhinal cortices in an age-dependent manner (Saiz-Sanchez et al., 2012). In APP$_{751SL}$/PS1$_{M146L}$ mice, a prominent decrease of CR-positive interneurons in CA1 and C2/3 hippocampal subfields has been reported already at 4 months of age (Baglietto-Vargas et al., 2010). Other studies have shown reductions in the numbers of interneurons expressing calcium-binding proteins such as CR or PV in the hippocampus of several AD mouse models, albeit at various
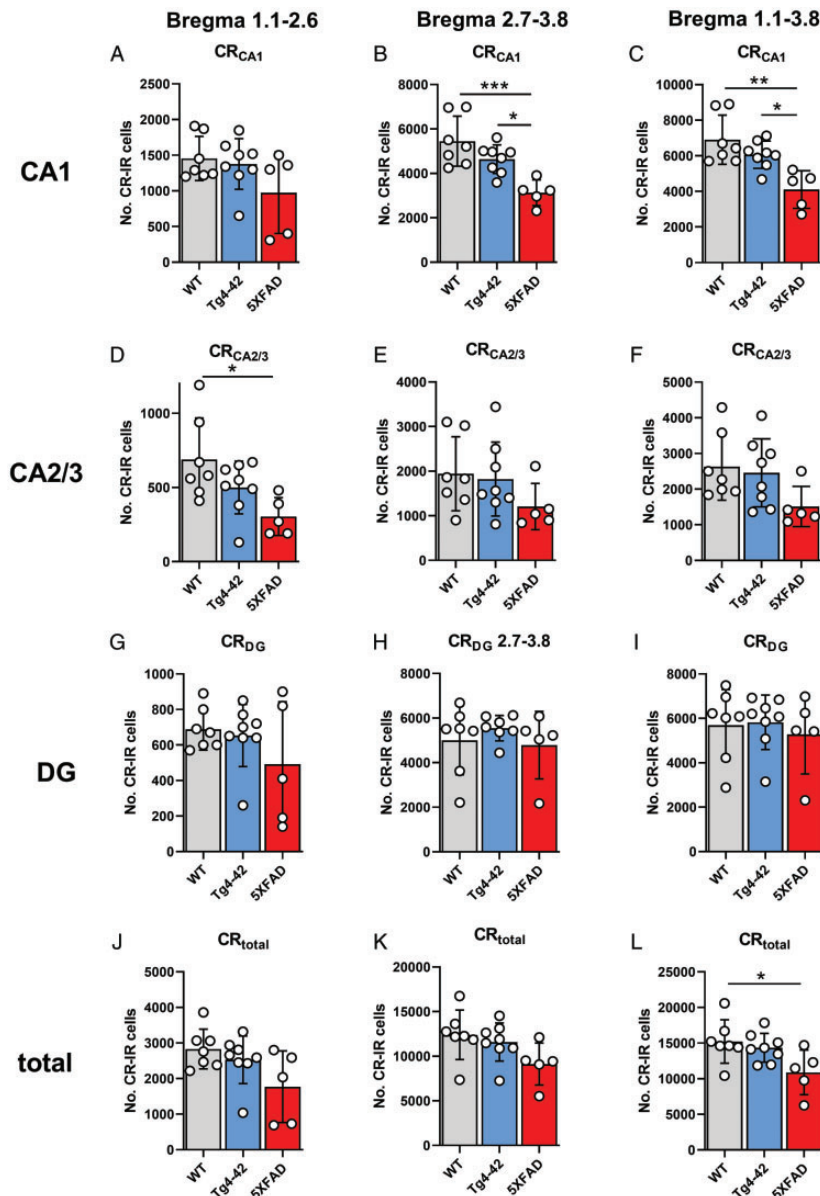
Figure 3. Quantification of CR-immunopositive cells in the hippocampal subfields CA1 (A to C), CA2/3 (D to F), DG (G to I), and the entire hippocampal formation (J to L). All graphs show mean ± standard deviation ($n = 5–8$ per group); $*p < .05$; $**p < .01$; $***p < .001$. CR = calretinin; IR = immunoreactive; WT =wild-type; DG = dentate gyrus.

ages and to a variable degree. APP$_{695swe}$/PS1$_{A246E}$ mice at 14 months of age showed a significant loss of both CR- and PV-positive cells in the DG with most prominent reductions in the polymorphic layer (Popović et al., 2008). In 6-month-old TgCRND8 mice, somatostatin-, neuropeptide Y (NPY)-, and PV-positive were quantified, demonstrating a loss of mainly neuropeptide Y-positive cells in a variety of hippocampal subregions, with PV neurons being only significantly reduced in the stratum oriens of CA3 (Albuquerque et al., 2015). On the other hand, significant reductions in PV-positive cells were reported in the CA1/2 layer and subiculum in the

same mouse line already at 1 month of age, a time point prior to amyloid plaque deposition (Mahar et al., 2017). 3xTg mice at 18 months of age showed a decrease of CR- and PV-positive cells in the CA1 layer of ∼33% and ∼52%, respectively (Zallo et al., 2018), which is in the range observed in the current study (∼40% for both CR and PV in the CA1). Neuroimaging studies provided evidence for a 10% decrease in hippocampal volume in 5XFAD mice compared with WT at 13 months of age (Macdonald et al., 2014). However, the observed reduction of CR- and PV-positive neuron numbers of ∼30% for CR- and more than 40% for PV-positive cells
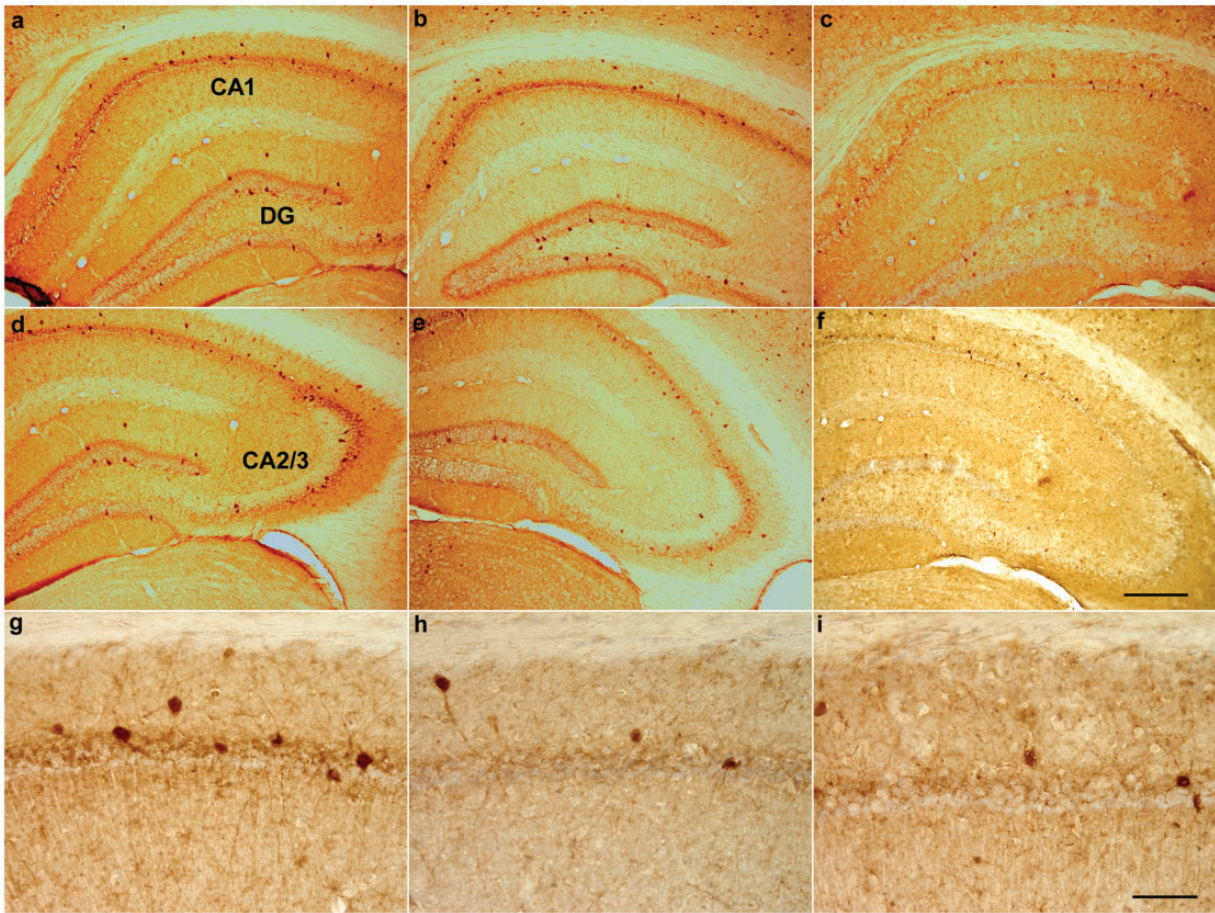
Figure 4. Distribution of parvalbumin (PV)-immunopositive cells within the hippocampal CA1, CA2/3, and DG subfields in 12-month-old WT (A, D), Tg4-42 (B, E), and 5XFAD mice (C, F). Higher magnifications of the CA1 layer in WT (G), Tg4-42 (H), and 5XFAD (I) mice. Scale bar: A to F: 200 μm; G to I: 50 μm.
DG = dentate gyrus.

suggests that volume loss alone is not sufficient to explain this observation. Takahashi et al. (2010) demonstrated significant reductions of PV- and CR-positive neurons in CA1/2 and DG in aged APP/PS1KI mice, an aggressive model that has been shown to harbor an ~50% loss of CA1 neurons and robust amyloid plaque pathology in brain regions such as cortex and hippocampus (Casas et al., 2004). Interestingly, no change in PV- and CR-positive neurons in Layers V and VI of the frontal cortex was detected in the latter model, although massive Thioflavin S-positive amyloid deposits were present, and pyramidal neurons were significantly reduced (>30%) in this cortical area (Lemmens et al., 2011).

It has been suggested that CR- and PV-containing interneurons, due to their abilities to effectively synchronize dendritic inhibitory interneurons and mediate lateral inhibition, play important roles in the hippocampal inhibitory network (Tóth and Maglóczky, 2014; Espinoza et al., 2018). An increased seizure risk has been reported in people with mild-to-moderate AD

(Amatniek et al., 2006), with an even higher incidence of epileptic activity in pedigrees carrying autosomal-dominant mutations (Palop and Mucke, 2009). Concerning this aspect, it is interesting that deficits in the levels of the voltage-gated sodium channel subunit Nav1.1, which is predominantly present in PV-expressing interneurons, have been linked to altered network activity and cognitive dysfunction in AD transgenic mice (Verret et al., 2012) but could be modulated by Nav1.1-overexpressing interneuron transplants (Martinez-Losa et al., 2018). Recent data indicate that treatment approaches aiming at preventing PV interneuron hyperexcitability might have long-term beneficial effects on memory and hippocampal network activity and might even result in reduced Aβ plaque deposition (Hijazi et al., 2019). We observed significantly reduced numbers of CR- and PV-positive cells in the hippocampus of plaque-bearing 5XFAD mice; however, no significant alterations compared with WT were measured in the Tg4-42 mouse model. While no data on epileptic
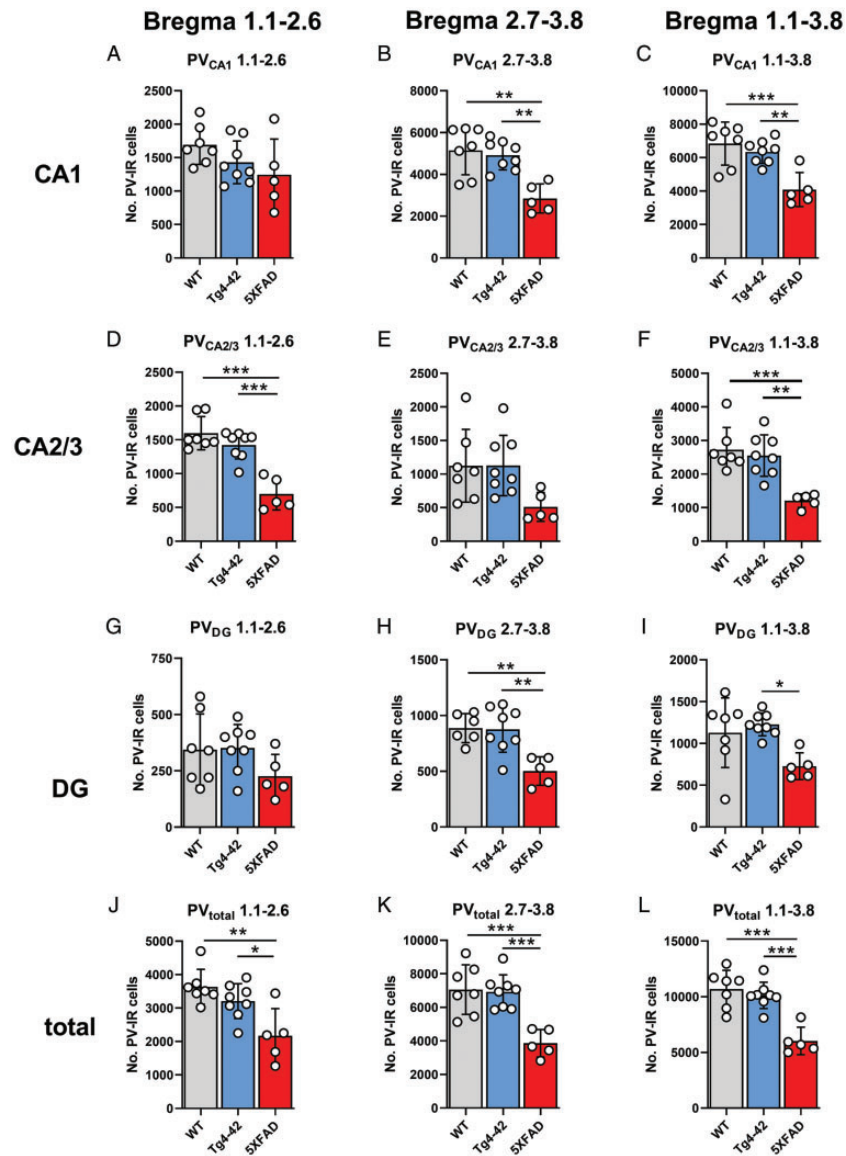
Figure 5. Quantification of PV-immunopositive cells in the hippocampal subfields CA1 (A to C), CA2/3 (D to F), DG (G to I), and the entire hippocampal formation (J to L). All graphs show mean ± standard deviation ($n = 5$–8 per group); *$p < .05$; **$p < .01$; ***$p < .001$. PV = parvalbumin; IR = immunoreactive; WT = wild-type; DG = dentate gyrus.
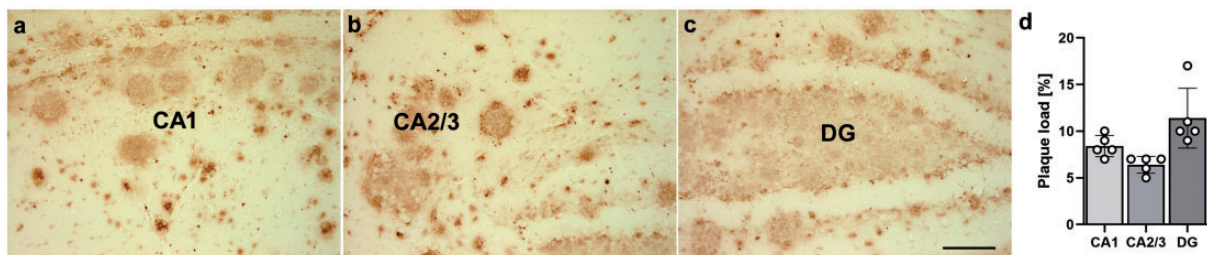
Figure 6. Quantification of amyloid plaque pathology in the hippocampus of 12-month-old 5XFAD mice ($n = 5$) using an antibody detecting pan-Aβ (4G8) (A to D). Representative images were shown. Scale bar: A to C: 100 μm. DG = dentate gyrus.

activity are available for the latter model, nonconvulsive seizures and reduced main theta frequencies have been reported in aged 5XFAD mice using simultaneous video-electroencephalogram monitoring (Paesler et al., 2015; Siwek et al., 2015). In addition, electroencephalogram recordings in 6-month-old male 5XFAD mice revealed a decrease of delta, theta, alpha, beta, and gamma frequency bands and a reduction of rapid eye movement sleep (Schneider et al., 2014). Epileptic activity was also observed in a fraction of TgCRND8 animals (Chishti et al., 2001), also showing increased sensitivity to pentylenetetrazole-induced seizures with a more severe seizure type over age-matched littermate controls (Del Vecchio et al., 2004). In the 3xTg mouse model, presenting with considerable loss of CR- and PV-positive neurons in the hippocampus (Zallo et al., 2018), audiogenic seizures were elicited in a higher proportion in young presymptomatic mice compared with age-matched controls (Kazim et al., 2017). In addition, in 8- to 10-month-old 3xTg mice, spike-wave discharges were detected that correlated with impairments in spatial memory. These spike-wave discharges could be suppressed using brivaracetam (Nygaard et al., 2015), an antiepileptic drug that binds synaptic vesicle protein 2A with high affinity (Gillard et al., 2011). Interestingly, sub-threshold stimulation using the kindling model revealed that synaptic vesicle protein 2A expression is specifically elevated in GABAergic interneurons of the DG. This is suggestive of a compensatory response by facilitating inhibitory GABAergic neurotransmission (Ohno et al., 2012), which might provide a mechanistic link between the loss of interneurons in the aforementioned models including 5XFAD and the observed increase in seizure susceptibility. Elevated comorbidity of epilepsy in AD has been observed, especially in familial AD cases with autosomal-dominant *APP* or *PSEN* mutations (Palop and Mucke, 2009; Noebels, 2011), with an increased risk in all age groups compared with the standard population and an up to >80-fold increase in the youngest group analyzed (age 50–59 years; Amatniek et al., 2006).

The loss of, in particular, PV-positive interneurons could be potentially linked to the loss of other neuron populations such as pyramidal cells, due to missing innervation (Roselli and Caroni, 2015); however, the repeatedly described massive CA1 pyramidal cell loss of >50% in aged heterozygous Tg4-42 mice (Supplemental Figure 1; Bouter et al., 2013; Hüttenrauch, Brauss et al., 2016) makes such a mechanism unlikely. In contrast, the observed interneuron loss in 5XFAD but not Tg4-42 might support previous observations linking the loss of CR-interneurons to the appearance of extracellular Aβ deposits and the formation of dystrophic neurites (Baglietto-Vargas et al., 2010). One of the limitations of the current study is a lack of longitudinal data and the small sample size of the 5XFAD group, which precludes

to establish clear-cut correlations between interneuron loss and amyloid plaque burden. Another limitation is a lack of information on gender differences, as only female mice have been employed in the current study. It is known that both 5XFAD on a C57Bl6/SJL hybrid background (Devi et al., 2010), as well as on a C57Bl6 congenic background, as used in the current study, show gender differences with a more rapid and more abundant amyloid pathology in female mice (Manji et al., 2019).

In conclusion, we provide evidence for significant reductions in CR- and PV-positive interneuron populations in the hippocampus of aged 5XFAD but not Tg4-42 mice. Although the latter model harbors extensive loss of CA1 pyramidal neurons, the lack of overt extracellular amyloid plaque pathology in contrast to the 5XFAD model might explain the preservation of these important hippocampal inhibitory cell types.

ORCID iD

Oliver Wirths 🔟 https://orcid.org/0000-0002-4115-0334

Supplemental Material

Supplemental material for this article is available online.

References

Albuquerque, M. S., Mahar, I., Davoli, M. A., Chabot, J.-G., Mechawar, N., Quirion, R., & Krantic, S. (2015). Regional and sub-regional differences in hippocampal GABAergic neuronal vulnerability in the TgCRND8 mouse model of Alzheimer's disease. *Front Aging Neurosci*, 7, 30.

Ali, F., Baringer, S. L., Neal, A., Choi, E. Y., & Kwan, A. C. (2019). Parvalbumin-positive neuron loss and amyloid-beta deposits in the frontal cortex of Alzheimer's disease-related mice. *J Alzheimers Dis*, 72(4), 1323–1339.

Amatniek, J. C., Hauser, W. A., DelCastillo-Castaneda, C., Jacobs, D. M., Marder, K., Bell, K., Albert, M., Brandt, J., & Stern, Y. (2006). Incidence and predictors of seizures in patients with Alzheimer's disease. *Epilepsia*, 47(5), 867–872.

Baglietto-Vargas, D., Moreno-Gonzalez, I., Sanchez-Varo, R., Jimenez, S., Trujillo-Estrada, L., Sanchez-Mejias, E., Torres, M., Romero-Acebal, M., Ruano, D., Vizuete, M., Vitorica, J., & Gutierrez, A. (2010). Calretinin interneurons are early targets of extracellular amyloid-beta pathology in PS1/

AbetaPP Alzheimer mice hippocampus. *J Alzheimers Dis*, *21*(1), 119–132.

Bouter, Y., Dietrich, K., Wittnam, J. L., Rezaei-Ghaleh, N., Pillot, T., Papot-Couturier, S., Lefebvre, T., Sprenger, F., Wirths, O., Zweckstetter, M., & Bayer, T. A. (2013). N-truncated amyloid beta (Abeta) 4-42 forms stable aggregates and induces acute and long-lasting behavioral deficits. *Acta Neuropathol*, *126*(2), 189–205.

Brady, D. R., & Mufson, E. J. (1997). Parvalbumin-immunoreactive neurons in the hippocampal formation of Alzheimer's diseased brain. *Neuroscience*, *80*(4), 1113–1125.

Casas, C., Sergeant, N., Itier, J. M., Blanchard, V., Wirths, O., van der Kolk, N., Vingtdeux, V., van de Steeg, E., Ret, G., Canton, T., Drobecq, H., Clark, A., Bonici, B., Delacourte, A., Benavides, J., Schmitz, C., Tremp, G., Bayer, T. A., Benoit, P., & Pradier, L. (2004). Massive CA1/2 neuronal loss with intraneuronal and N-terminal truncated Abeta42 accumulation in a novel Alzheimer transgenic model. *Am J Pathol*, *165*(4), 1289–1300.

Chishti, M. A., et al. (2001). Early-onset amyloid deposition and cognitive deficits in transgenic mice expressing a double mutant form of amyloid precursor protein 695. *J Biol Chem*, *276*(24), 21562–21570.

Cotel, M. C., Bayer, T. A., & Wirths, O. (2008). Age-dependent loss of dentate gyrus granule cells in APP/PS1KI mice. *Brain Res*, *1222*, 207–213.

Del Vecchio, R. A., Gold, L. H., Novick, S. J., Wong, G., & Hyde, L. A. (2004). Increased seizure threshold and severity in young transgenic CRND8 mice. *Neurosci Lett*, *367*(2), 164–167.

Devi, L., Alldred, M. J., Ginsberg, S. D., & Ohno, M. (2010). Sex- and brain region-specific acceleration of beta-amyloidogenesis following behavioral stress in a mouse model of Alzheimer's disease. *Mol Brain*, *3*, 34.

Espinoza, C., Guzman, S. J., Zhang, X., & Jonas, P. (2018). Parvalbumin+ interneurons obey unique connectivity rules and establish a powerful lateral-inhibition microcircuit in dentate gyrus. *Nat Commun*, *9*(1), 4605.

Flanigan, T. J., Xue, Y., Kishan Rao, S., Dhanushkodi, A., & McDonald, M. P. (2014). Abnormal vibrissa-related behavior and loss of barrel field inhibitory neurons in 5xFAD transgenics. *Genes Brain Behav*, *13*(5), 488–500.

Gerberding, A. L., Zampar, S., Stazi, M., Liebetanz, D., & Wirths, O. (2019). Physical activity ameliorates impaired hippocampal neurogenesis in the Tg4-42 mouse model of Alzheimer's disease. *ASN Neuro*, *11*, 1759091419892692.

Gillard, M., Fuks, B., Leclercq, K., & Matagne, A. (2011). Binding characteristics of brivaracetam, a selective, high affinity SV2A ligand in rat, mouse and human brain: Relationship to anti-convulsant properties. *Eur J Pharmacol*, *664*(1), 36–44.

Gulyás, A. I., Hájos, N., & Freund, T. F. (1996). Interneurons containing calretinin are specialized to control other interneurons in the rat hippocampus. *J Neurosci*, *16*(10), 3397–3411.

Hijazi, S., Heistek, T. S., Scheltens, P., Neumann, U., Shimshek, D. R., Mansvelder, H. D., Smit, A. B., & van Kesteren, R. E. (2019). Early restoration of parvalbumin interneuron activity prevents memory loss and network hyperexcitability in a mouse model of Alzheimer's disease. *Mol Psychiatry*. Advance online publication. https://doi.org/10.1038/s41380-019-0483-4

Hu, H., Gan, J., & Jonas, P. (2014). Fast-spiking, parvalbumin-positive GABAergic interneurons: From cellular design to microcircuit function. *Science*, *345*(6196), 1255263.

Hüttenrauch, M., Brauss, A., Kurdakova, A., Borgers, H., Klinker, F., Liebetanz, D., Salinas-Riester, G., Wiltfang, J., Klafki, H. W., & Wirths, O. (2016). Physical activity delays hippocampal neurodegeneration and rescues memory deficits in an Alzheimer disease mouse model. *Transl Psych*, *6*, e800.

Hüttenrauch, M., Salinas, G., & Wirths, O. (2016). Effects of long-term environmental enrichment on anxiety, memory, hippocampal plasticity and overall brain gene expression in C57BL6 mice. *Front Mol Neurosci*, *9*, 62.

Hüttenrauch, M., Walter, S., Kaufmann, M., Weggen, S., & Wirths, O. (2017). Limited effects of prolonged environmental enrichment on the pathology of 5XFAD mice. *Mol Neurobiol*, *54*(8), 6542–6555.

Jawhar, S., Trawicka, A., Jenneckens, C., Bayer, T. A., & Wirths, O. (2012). Motor deficits, neuron loss, and reduced anxiety coinciding with axonal degeneration and intraneuronal Abeta aggregation in the 5XFAD mouse model of Alzheimer's disease. *Neurobiol Aging*, *33*(1), 196.e129–196.e140.

Kazim, S. F., Chuang, S.-C., Zhao, W., Wong, R. K. S., Bianchi, R., & Iqbal, K. (2017). Early-onset network hyperexcitability in presymptomatic Alzheimer's disease transgenic mice is suppressed by passive immunization with anti-human APP/Aβ antibody and by mGluR5 blockade. *Front Aging Neurosci*, *9*, 71).

Klausberger, T., Marton, L. F., O'Neill, J., Huck, J. H. J., Dalezios, Y., Fuentealba, P., Suen, W. Y., Papp, E., Kaneko, T., Watanabe, M., Csicsvari, J., & Somogyi, P. (2005). Complementary roles of cholecystokinin- and parvalbumin-expressing GABAergic neurons in hippocampal network oscillations. *J Neurosci*, *25*(42), 9782–9793.

Lemmens, M. A., Sierksma, A. S., Rutten, B. P., Dennissen, F., Steinbusch, H. W., Lucassen, P. J., & Schmitz, C. (2011). Age-related changes of neuron numbers in the frontal cortex of a transgenic mouse model of Alzheimer's disease. *Brain Struct Funct*, *216*(3), 227–237.

Leuba, G., Kraftsik, R., & Saini, K. (1998). Quantitative distribution of parvalbumin, calretinin, and calbindin D-28k immunoreactive neurons in the visual cortex of normal and Alzheimer cases. *Exp Neurol*, *152*(2), 278–291.

Macdonald, I. R., DeBay, D. R., Reid, G. A., O'Leary, T. P., Jollymore, C. T., Mawko, G., Burrell, S., Martin, E., Bowen, C. V., Brown, R. E., & Darvesh, S. (2014). Early detection of cerebral glucose uptake changes in the 5XFAD mouse. *Curr Alzheimer Res*, *11*(5), 450–460.

Mahar, I., Albuquerque, M. S., Mondragon-Rodriguez, S., Cavanagh, C., Davoli, M. A., Chabot, J.-G., Williams, S., Mechawar, N., Quirion, R., & Krantic, S. (2017). Phenotypic alterations in hippocampal NPY- and PV-expressing interneurons in a presymptomatic transgenic mouse model of Alzheimer's *disease*. *Front Aging Neurosci*, *8*, 327.

Manji, Z., Rojas, A., Wang, W., Dingledine, R., Varvel, N. H., & Ganesh, T. (2019). 5xFAD mice display sex-dependent inflammatory gene induction during the prodromal stage of Alzheimer's disease. *J Alzheimers Dis*, *70*(4), 1259–1274.

Martinez-Losa, M., Tracy, T. E., Ma, K., Verret, L., Clemente-Perez, A., Khan, A. S., Cobos, I., Ho, K., Gan, L., Mucke, L., Alvarez-Dolado, M., & Palop, J. J. (2018). Nav1.1-over-expressing interneuron transplants restore brain rhythms and cognition in a mouse model of Alzheimer's disease. *Neuron*, *98*(1), 75–89.e75.

Mikkonen, M., Alafuzoff, I., Tapiola, T., Soininen, H., & Miettinen, R. (1999). Subfield- and layer-specific changes in parvalbumin, calretinin and calbindin-D28k immunoreactivity in the entorhinal cortex in Alzheimer's disease. *Neuroscience*, *92*(2), 515–532.

Noebels, J. (2011). A perfect storm: Converging paths of epilepsy and Alzheimer's dementia intersect in the hippocampal formation. *Epilepsia*, *52*(s1), 39–46.

Nygaard, H. B., Kaufman, A. C., Sekine-Konno, T., Huh, L. L., Going, H., Feldman, S. J., Kostylev, M. A., & Strittmatter, S. M. (2015). Brivaracetam, but not ethosuximide, reverses memory impairments in an Alzheimer's disease mouse model. *Alzheimers Res Ther*, *7*(1), 25.

Oakley, H., Cole, S. L., Logan, S., Maus, E., Shao, P., Craft, J., Guillozet-Bongaarts, A., Ohno, M., Disterhoft, J., Van Eldik, L., Berry, R., & Vassar, R. (2006). Intraneuronal beta-amyloid aggregates, neurodegeneration, and neuron loss in transgenic mice with five familial Alzheimer's disease mutations: Potential factors in amyloid plaque formation. *J Neurosci*, *26*(40), 10129–10140.

Ohno, Y., Okumura, T., Terada, R., Ishihara, S., Serikawa, T., & Sasa, M. (2012). Kindling-associated SV2A expression in hilar GABAergic interneurons of the mouse dentate gyrus. *Neurosci Lett*, *510*(2), 93–98.

Paesler, K., Xie, K., Hettich, M. M., Siwek, M. E., Ryan, D. P., Schroder, S., Papazoglou, A., Broich, K., Muller, R., Trog, A., Garthe, A., Kempermann, G., Weiergraber, M., & Ehninger, D. (2015). Limited effects of an eIF2alphaS51A allele on neurological impairments in the 5xFAD mouse model of Alzheimer's disease. *Neural Plast*, *2015*, 825157.

Palop, J. J., & Mucke, L. (2009). Epilepsy and cognitive impairments in Alzheimer disease. *Arch Neurol*, *66*(4), 435–440.

Paxinos, G., & Franklin, K. B. J. (2001). *The mouse brain in stereotaxic coordinates*. Academic Press.

Pearson, R. C., Esiri, M. M., Hiorns, R. W., Wilcock, G. K., & Powell, T. P. (1985). Anatomical correlates of the distribution of the pathological changes in the neocortex in Alzheimer disease. *Proc Nat Acad Sci*, *82*(13), 4531–4534.

Pelkey, K. A., Chittajallu, R., Craig, M. T., Tricoire, L., Wester, J. C., & McBain, C. J. (2017). Hippocampal GABAergic inhibitory interneurons. *Physiol Rev*, *97*(4), 1619–1747.

Popović, M., Caballero-Bleda, M., Kadish, I., & Van Groen, T. (2008). Subfield and layer-specific depletion in calbindin-D28K, calretinin and parvalbumin immunoreactivity in the dentate gyrus of amyloid precursor protein/presenilin 1 transgenic mice. *Neuroscience*, *155*(1), 182–191.

Portelius, E., Bogdanovic, N., Gustavsson, M. K., Volkmann, I., Brinkmalm, G., Zetterberg, H., Winblad, B., & Blennow, K. (2010). Mass spectrometric characterization of brain amyloid beta isoform signatures in familial and sporadic Alzheimer's disease. *Acta Neuropathol*, *120*(2), 185–193.

Roselli, F., & Caroni, P. (2015). From intrinsic firing properties to selective neuronal vulnerability in neurodegenerative diseases. *Neuron*, *85*(5), 901–910.

Saiz-Sanchez, D., De la Rosa-Prieto, C., Ubeda-Banon, I., & Martinez-Marcos, A. (2015). Interneurons, tau and amyloid-β in the piriform cortex in Alzheimer's disease. *Brain Struct Funct*, *220*(4), 2011–2025.

Saiz-Sanchez, D., Ubeda-Banon, I., De la Rosa-Prieto, C., & Martinez-Marcos, A. (2012). Differential expression of interneuron populations and correlation with amyloid-beta deposition in the olfactory cortex of an AbetaPP/PS1 transgenic mouse model of Alzheimer's disease. *J Alzheimers Dis*, *31*(1), 113–129.

Sampson, V. L., Morrison, J. H., & Vickers, J. C. (1997). The cellular basis for the relative resistance of parvalbumin and calretinin immunoreactive neocortical neurons to the pathology of Alzheimer's disease. *Exp Neurol*, *145*(1), 295–302.

Sanchez-Mejias, E., Nuñez-Diaz, C., Sanchez-Varo, R., Gomez-Arboledas, A., Garcia-Leon, J. A., Fernandez-Valenzuela, J. J., Mejias-Ortega, M., Trujillo-Estrada, L., Baglietto-Vargas, D., Moreno-Gonzalez, I., Davila, J. C., Vitorica, J., & Gutierrez, A. (2020). Distinct disease-sensitive GABAergic neurons in the perirhinal cortex of Alzheimer's mice and patients. *Brain Pathol*, *30*(2), 345–363.

Schneider, F., Baldauf, K., Wetzel, W., & Reymann, K. G. (2014). Behavioral and EEG changes in male 5xFAD mice. *Physiol Behav*, *135*(0), 25–33.

Selkoe, D. J. (2001). Alzheimer's disease: Genes, proteins, and therapy. *Physiol Rev*, *81*(2), 741–766.

Siwek, M. E., Muller, R., Henseler, C., Trog, A., Lundt, A., Wormuth, C., Broich, K., Ehninger, D., Weiergraber, M., & Papazoglou, A. (2015). Altered theta oscillations and aberrant cortical excitatory activity in the 5XFAD model of Alzheimer's disease. *Neural Plast*, *2015*, 781731.

Takahashi, H., Brasnjevic, I., Rutten, B. P., Van Der Kolk, N., Perl, D. P., Bouras, C., Steinbusch, H. W., Schmitz, C., Hof, P. R., & Dickstein, D. L. (2010). Hippocampal interneuron loss in an APP/PS1 double mutant mouse and in Alzheimer's disease. *Brain Struct Funct*, *214*(2–3), 145–160.

Tóth, K., & Maglóczky, Z. (2014). The vulnerability of calretinin-containing hippocampal interneurons to temporal lobe epilepsy. *Front Neuroanat*, *8*, 100.

Verdaguer, E., Brox, S., Petrov, D., Olloquequi, J., Romero, R., de Lemos, M. L., Camins, A., & Auladell, C. (2015). Vulnerability of calbindin, calretinin and parvalbumin in a transgenic/knock-in APPswe/PS1dE9 mouse model of Alzheimer disease together with disruption of hippocampal neurogenesis. *Exp Gerontol*, *69*, 176–188.

Verret, L., Mann, E. O., Hang, G. B., Barth, A. M., Cobos, I., Ho, K., Devidze, N., Masliah, E., Kreitzer, A. C., Mody, I., Mucke, L., & Palop, J. J. (2012). Inhibitory interneuron deficit links altered network activity and cognitive dysfunction in Alzheimer model. *Cell*, *149*(3), 708–721.

Wirths, O., Multhaup, G., Czech, C., Feldmann, N., Blanchard, V., Tremp, G., Beyreuther, K., Pradier, L., & Bayer, T. A. (2002). Intraneuronal APP/A beta trafficking and plaque

formation in beta-amyloid precursor protein and presenilin-1 transgenic mice. *Brain Pathol*, *12*(3), 275–286.

Wirths, O., & Zampar, S. (2019). Emerging roles of N- and C-terminally truncated Aβ species in Alzheimer's disease. *Expert Opin Ther Targets*, *23*(12), 991–1004.

Xia, F., Richards, B. A., Tran, M. M., Josselyn, S. A., Takehara-Nishiuchi, K., & Frankland, P. W. (2017).

Parvalbumin-positive interneurons mediate neocortical-hippocampal interactions that are necessary for memory consolidation. *eLife*, *6*, e27868.

Zallo, F., Gardenal, E., Verkhratsky, A., & Rodríguez, J. J. (2018). Loss of calretinin and parvalbumin positive interneurones in the hippocampal CA1 of aged Alzheimer's disease mice. *Neurosci Lett*, *681*, 19–25.